MAGNONICS

Mutual control of coherent spin waves and magnetic domain walls in a magnonic device

Jiahao Han, Pengxiang Zhang, Justin T. Hou, Saima A. Siddiqui, Luqiao Liu*

The successful implementation of spin-wave devices requires efficient modulation of spin-wave propagation. Using cobalt/nickel multilayer films, we experimentally demonstrate that nanometer-wide magnetic domain walls can be applied to manipulate the phase and magnitude of coherent spin waves in a nonvolatile manner. We further show that a spin wave can, in turn, be used to change the position of magnetic domain walls by means of the spin-transfer torque effect generated from magnon spin current. This mutual interaction between spin waves and magnetic domain walls opens up the possibility of realizing all-magnon spintronic devices, in which one spin-wave signal can be used to control others by reconfiguring magnetic domain structures.

As propagating oscillations of magnetic moments, spin waves (SWs) can transmit spin information over macroscopic distances in the absence of Joule heating (*1*–*6*). To manipulate the propagation of SWs, various methods such as lithographically defined synthetic crystals (*7*, *8*), static magnetic fields (*9*, *10*), and electrical currents (*11*–*14*) have been used. The large size (above the micrometer scale) of control terminals and high power consumption in these devices pose obstacles for practical applications. Magnetic textures such as magnetic domain walls (DWs) have been suggested as an alternative. It has been predicted that DWs can cause substantial changes in the phase and magnitude of SWs within the length scale of nanometers (*15*–*19*). This prediction, in combination with reconfigurability (*20*, *21*) and nonvolatility (*22*) of DWs, makes DWs promising candidates for modulating SWs. However, little experimental progress has been reported in this direction (*23*). A major challenge for experimentally studying the SW transmission in the presence of DWs is that resonant excitation and coherent propagation of SWs require well-defined quantization axes for spins. In existing studies, this condition is usually realized through the application of a large external magnetic field (*8*–*10*, *12*–*14*), which prevents the formation of more than one magnetic domain. To achieve the coexistence of DWs and zero-field ferromagnetic resonance (FMR), thin films with strong magnetic anisotropy and low damping are highly desirable. In addition to DW-modulated SW transmission, the mutual interactions between SWs and DWs can enable the inverse effect: the SW-induced DW movement. As shown in Fig. 1A, SWs carry magnon spin currents along their propagation direction. On the two sides of a DW, the magnons have opposite spin angular momentum and flow in the same direction, leading to a net spin injection into the DW. This provides the possibility of manipulating the orientation of magnetic domains through magnon-induced spin-transfer torque (*24*).

In this study, we employed magnetic films with perpendicular magnetic anisotropy (PMA) to achieve the mutual control of SWs and DWs. The magnetic films used in our experiments consist of substrate/Ti(8)/Pt(7)/$[Co(0.4)/Ni(0.35\sim0.4)]_9$/Ru(3) (numbers indicate width in nanometers). The Co/Ni multilayer films were chosen for their high PMA, large magnetic volume, and low magnetic damping. Different from other films with interfacial PMA such as Ta/CoFeB/MgO or Pt/Co/AlO_x, in which only one thin layer of magnetic material can be used to carry SWs, our perpendicularly magnetized Co/Ni multilayers (*25*) have a much larger total magnetic thickness, carrying larger amounts of power through SWs. In addition, Co/Ni films exhibit moderate magnetic damping (*26*) compared with other bulk PMA films, enabling propagation of SWs over detectable distances. FMR spectra (Fig. 1B) were obtained on an unpatterned film by sweeping the field with fixed microwave frequency, and a moderate Gilbert damping factor of 0.024 was determined (Fig. 1C) (*25*). Moreover, a zero-field FMR was reached at 7.5 GHz (Fig. 1B), which made it possible to excite coherent SWs while maintaining the DW structure.

To study the SW propagation, we patterned films into strips with width between 3 and 6 μm and then deposited SiO_2 mesas (50 nm thick) for electrical isolation. A pair of microwave antennae was further deposited for SW excitation and detection (*27*, *28*). Following the design in (*28*), we fabricated the antennae as ground-signal-ground coplanar waveguides with three meanders to obtain a well-defined wavelength (3.2 μm) corresponding to a wave number of $k = 1.96\ \mu m^{-1}$ (Fig. 2, A and B). This design ensures the resonant generation of highly coherent SWs with more uniform wavelength, in contrast to other approaches that use thermal gradient (*29*), spin injection (*6*, *30*), or broadband microstrip (*9*, *10*, *12*) to excite SWs. The excitation and transmission of SWs were monitored with a 20-GHz vector network analyzer through the *S*-parameter measurement. The spectra of microwave reflection coefficient S_{11} and transmission coefficient S_{21} of a uniformly magnetized channel at zero dc field are shown in Fig. 2C and the upper trace of Fig. 2D, respectively; both exhibit resonant features at 7.8 GHz. To verify the magnetic origin of the observed resonant signal, we measured S_{21} spectra under different applied external fields H_{ext}, with the resonant frequency f versus H_{ext} relationship summarized in the inset of Fig. 2D. A typical spectrum at H_{ext} = 200 Oe is shown as the bottom trace in Fig. 2D. The oscillating real and imaginary parts with a 90° phase difference are typical characteristics of propagating SWs. In a control sample with a 2.6-μm-wide gap in the magnetic strip between two antennae (inset of Fig. 2E), no transmission signal was detected within the resolution of our setup (Fig. 2E). Moreover, S_{21} spectra with different propagation lengths were measured, for which the SW decay length (*31*) of ~3 μm was extracted and the propagating SW picture was further confirmed (fig. S3).

We then studied the transmission of SWs through a DW by using microwave circuits integrated with a magneto-optic Kerr effect (MOKE) microscope (Fig. 3A). Figure 3, B and C, shows typical MOKE images, with bright and dark colors representing oppositely oriented domains. By applying millisecond magnetic field pulses, we toggled the magnetic strip between a uniformly magnetized state (Fig. 3B) and a DW state (Fig. 3C). The DW width is estimated to be ~20 nm (*25*). During the measurement, the edge of the SiO_2 mesa assists the pinning of the DW, allowing for repeatable formation of DWs at the same location. By comparing the S_{21} spectra that correspond to the two different magnetic states in Fig. 3, B and C (Fig. 3, D and E, respectively), we found that when SWs pass through a DW, they keep the same resonance frequency as the uniform state but experience a magnitude attenuation by a factor of 4.3 (or, equivalently, a power reduction by a factor of 18). This observed reduction in the transmitted SW magnitude is consistent with the previous experiment on more complicated Landau domain structures (*23*), which can be explained by the reflection of SWs at the DW edge caused by the quasi-rigid boundary condition for magnetic moments. Aside from the attenuation in magnitude, a 175° phase shift appears for the SWs propagating through the DW (see the real and imaginary parts of S_{21} in Fig. 3, D and E). This nearly 180° phase shift is robust across our fabricated devices and immune to specific DW configuration (i.e., up-down or down-up). Five devices with the same design

Department of Electrical Engineering and Computer Science, Massachusetts Institute of Technology, Cambridge, MA 02139, USA.
*Corresponding author. Email: luqiao@mit.edu

have been checked and similar results have been obtained, with variance of the magnitude attenuation and the phase shift being within 10% (figs. S5 and S6). Control of wave phases lies at the heart of physical implementation of wave-based computing and signal processing. Various magnonic logic devices (*4*, *15*, *19*, *32*), which rely on the interference between SWs with different phases, have been previously proposed. The experimental discovery of the phase-shifting effect can therefore be useful for realizing those devices.

To better understand the DW-induced SW modulation, we carried out micromagnetic simulations (*33*) by using material parameters consistent with our real samples. Figure 3F presents the top view of a magnetic channel with propagating SWs, described by the x component of magnetization (m_x). We chose to monitor m_x in the simulations because of its direct correlation with the experimental observable in our sample geometry (*25*). A radio frequency magnetic field was locally applied near one end of the channel to excite SWs. Considering the magnetostatic nature of our SW, we set the aspect ratio between the channel width and the SW wavelength to be the same as that of the real device. By comparing the top and bottom panels of Fig. 3F, it is evident that when the SWs encounter a DW, the oscillating m_x experiences an attenuation in magnitude and a shift of ~180° in phase, consistent with our experimental results. The phase shift in the narrow DW limit can also be possibly explained by considering the magnetic field boundary conditions at the opposite ends of the DW (*25*).

Similar to spin-valve structures, in which magnetic orientation may result in resistance change (giant or tunneling magnetoresistance) and current may induce magnetic switching (spin-transfer torque), the device structure studied in our experiments can also exhibit this pair of inverse effects. In the structure shown in Fig. 1A, the SWs carry magnon spin current J_s with spin angular momentum antiparallel to the local equilibrium direction. Across the DW, the spins carried by J_s reverse sign, resulting in net spin current divergence, which can further cause spin-transfer torque–induced magnetic switching. To observe this effect experimentally, we applied large-magnitude SWs by increasing the driving microwave power. Moreover, we adopted a simple antenna design with one meander (Fig. 4A), whose reduced resistance optimizes the impedance matching with the microwave circuit. In addition, a single antenna, rather than antenna pairs, was employed for clearer observation of the DW movement at longer length scales. In this measurement, an up-down DW was nucleated close to the antenna with external magnetic field pulses, as shown by the boundary between the bright and dark regions

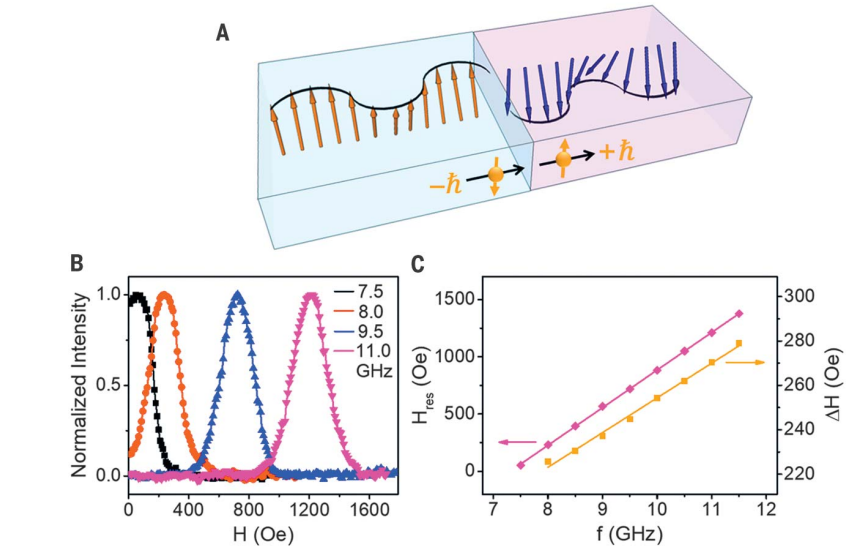

Fig. 1. Illustration of the basic concept and FMR measurements of thin-film samples. (**A**) Schematic of SWs passing through a DW. The magnons at different sides of the DW carry opposite spins, which leads to a spin angular momentum transfer to the DW. $\pm\hbar$ represents the angular momentum of each magnon. (**B**) FMR spectra of unpatterned Co/Ni films at different microwave frequencies. The field is applied out of plane. (**C**) FMR resonant field (H_{res}) and linewidth (ΔH) as a function of microwave frequency.

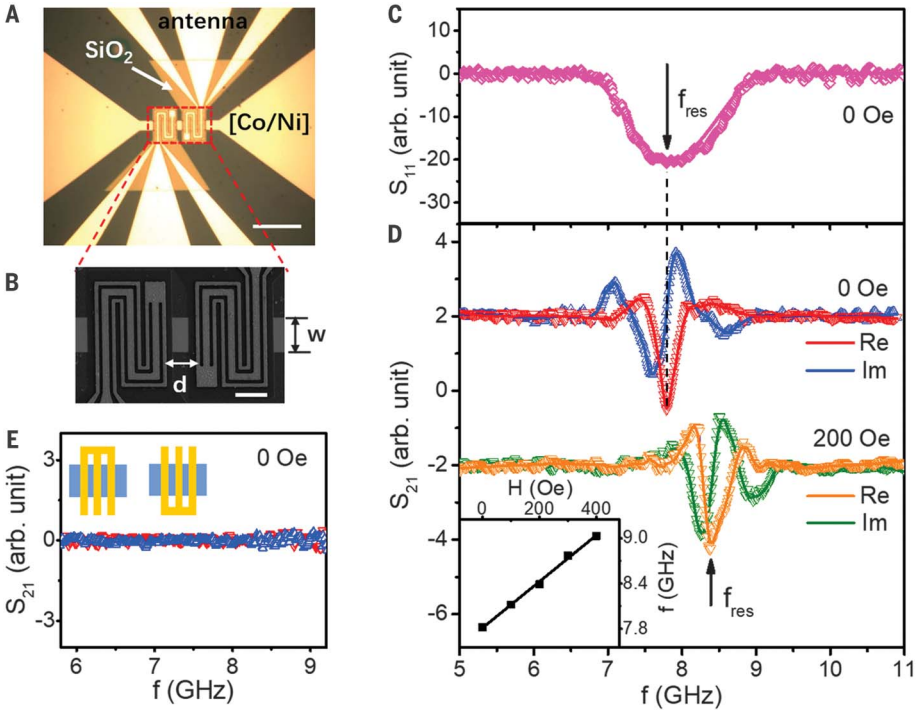

Fig. 2. SW transmission in uniformly magnetized devices. (**A**) Optical image of the device. Scale bar, 30 μm. (**B**) Scanning electron microscopy (SEM) image of the center of the device. The width of the magnetic channel is w = 6 μm and the distance between the antennae is d = 6.4 μm. Scale bar, 6 μm. (**C**) Reflection spectrum S_{11} at zero field. (**D**) Transmission spectrum S_{21} with external fields of 0 (top) and 200 Oe (bottom). The (arbitrary) unit is the same for S_{11} and S_{21}, enabling a comparison of their values. Re, real; Im, imaginary. (Inset) Resonant frequency as a function of external field measured from S_{21}. (**E**) Transmission spectrum of a control sample, where the magnetic strip is discontinuous with a 2.6-μm-wide gap between the antennae. A microwave power of 4 μW was used for all measurements depicted in this figure.

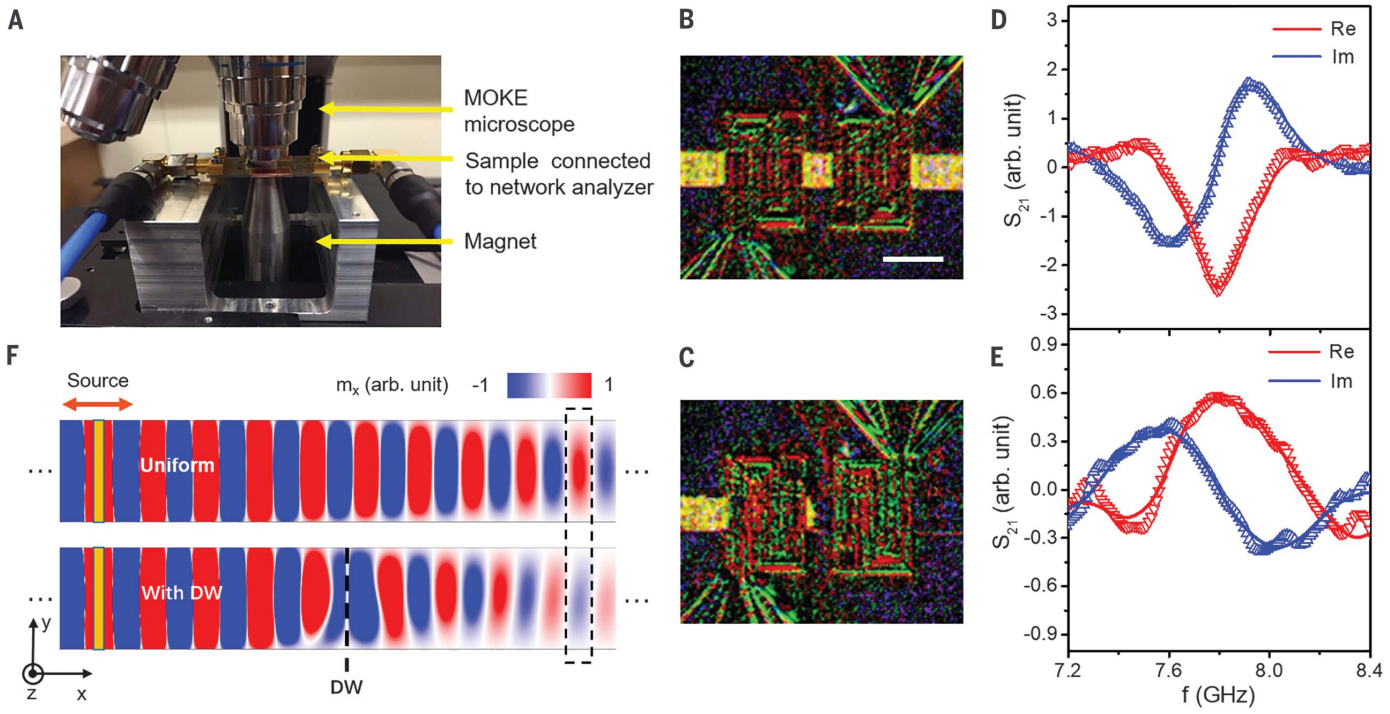

Fig. 3. SW propagation across a DW. (**A**) Photo of the experimental setup. (**B** and **C**) MOKE images of the device in a uniformly magnetized state and a DW state, respectively. The bright and dark regions in the magnetic channel represent domains with up and down magnetization. In the DW state, the wall is located between the two antennae. Scale bar, 10 μm. (**D** and **E**) S_{21} spectra for (B) and (C). A microwave power of 4 μW was used for the measurement. (**F**) Simulated SW propagation in a 600-nm-wide magnetic channel without (top) and with (bottom) a DW. The SW wavelength is 320 nm. m_x represents the *x* component of the magnetization. The dashed rectangle indicates a typical region for comparing the magnitude and phase of the transmitted SWs in the uniform channel and the channel with a DW.

in the top panel of Fig. 4B. With the application of the SW, the DW moves toward the SW source in the absence of any dc magnetic field and stops underneath the antenna (bottom panel of Fig. 4B). A similar effect was observed for the down-up DW (see the movement of the boundary between dark and bright regions in Fig. 4C). When the device was driven with off-resonance microwave signals at the same power, no DW motion was detected. In our experiment, DWs always move against the SW-flowing direction, consistent with the magnonic spin-transfer torque mechanism (*24*, *34*) and in contrast to the linear momentum transfer picture (*35*). This observed DW movement direction differs from the recently observed field-induced DW movement under the assistance of transient SWs (*36*), where SWs help DWs move along the wave-flowing direction. Using the microwave power in our DW motion experiment, we can estimate the spin current density carried by the SW to be on the order of $10^7(h/2e)\mathrm{A/cm}^2$ (h, Planck's constant divided by 2π; e, elementary charge) (*25*), similar to the typical threshold spin current density needed for current-induced DW motion (*22*). Under this magnon spin current density, the DW velocity is expected to be ~10 m/s (*24*, *25*), comparable to the velocities obtained in the spin-transfer torque configuration (*22*).

To further verify the spin-transfer torque origin of the observed DW motion, we experimentally determined the switching phase diagram of the DW under applied SW and external fields. The depinning field (H_{depin}) was measured by simultaneously applying external magnetic field pulses and continuous microwave power at the resonant frequency. Using the magnetometry mode of MOKE microscope, we determined the switching curves of magnetic domains (Fig. 4D). Under the application of SWs, H_{depin} exhibits an overall shift, indicating that the SWs assist the DW to move toward the antenna and hamper the motion in the opposite direction. H_{depin} as a function of the driving microwave power is summarized in Fig. 4E under both on-resonance frequency (8.8 GHz) and off-resonance frequency (7 GHz). For the off-resonance case, a simple reduction of H_{depin} in both directions was observed, which can be explained by a trivial thermal effect that suppresses the switching energy barrier. By comparing the slopes of the two groups of curves, we found that, whereas the thermal effects are similar, only the on-resonance data show asymmetries in H_{depin} of the two different switching directions, indicating that coherent magnons other than thermally induced spin flow (*29*) play a major role in the observed DW motion. To exclude the contribution from the extra heating effect caused by FMR, we used the anomalous Hall effect to quantitatively characterize the magnetization change in the two experimental situations, as well as to compare them with the change caused by dc current–induced Joule heating. We found that the heating-induced reduction in magnetization cannot account for the observed effect (*25*). Finally, H_{depin} under different driving frequencies is summarized in Fig. 4G, consistent with the SW absorption spectrum (Fig. 4F).

The transfer of spin current with magnon flow represents an energy-efficient process. To transfer one unit of spin angular momentum (h), the energy of a magnon ($h\omega$) must be consumed, corresponding to tens of micro–electron volts for gigahertz SWs. This amount is smaller than the energy consumption in other spin current–generation methods such as tunnel junctions or spin valves, for which the corresponding value is in the range of milli–electron volts to sub–electron volts. Substantial differences still exist between the power carried by the SW in the device and that generated at our microwave source, which mainly comes from the low efficiency associated with the inductive generation of SWs using the antenna, degrading the overall power performance of the studied device. This can be improved by using energy-efficient SW generation mechanisms (*37*, *38*). In the meantime, the energy

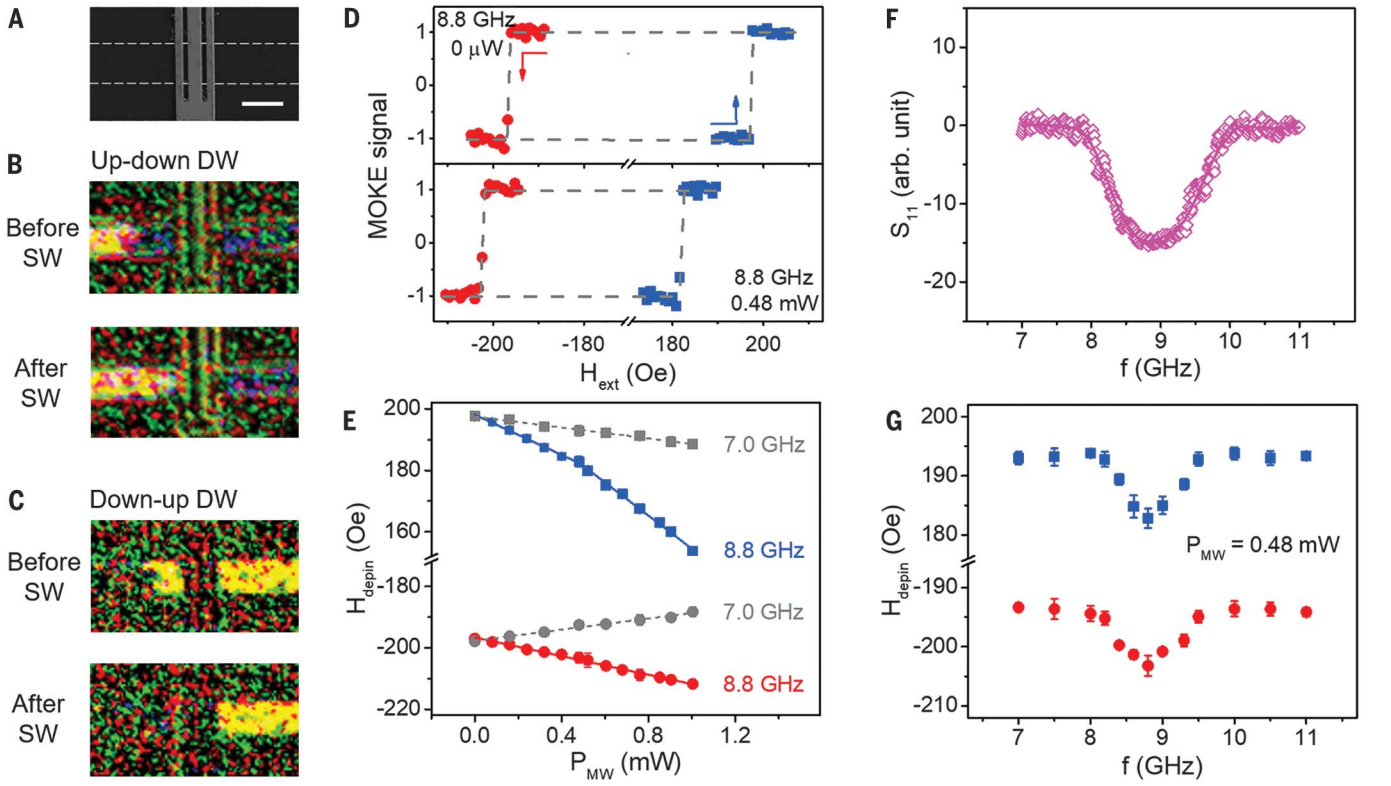

Fig. 4. Magnetic domain switching induced by SWs. (**A**) SEM image of the device. The magnetic strip under SiO_2 is marked by the dashed lines. Scale bar, 4 μm. (**B** and **C**) MOKE images showing the movement of the up-down and down-up DWs under zero dc magnetic field. The bright and dark regions in the magnetic channel represent domains with up and down magnetization. The microwave power applied onto the antenna is P_{MW} = 2.2 mW at resonant frequency (8.8 GHz for this sample, slightly higher than the previous value, owing to the stronger anisotropy field). See (*25*) for the power calibration methods. (**D**) Magnetic switching around the DW location measured from a MOKE magnetometer, under microwave power of P_{MW} = 0.48 mW at 8.8 GHz. (**E**) H_{depin} as a function of microwave power. (**F**) SW reflection spectrum at zero dc field. (**G**) H_{depin} as a function of microwave frequency. The microwave power is fixed at P_{MW} = 0.48 mW. The applied field in this measurement is small compared with the linewidth of this sample, so the SWs still propagate across the DW with slightly reduced power.

efficiency of magnonic devices can be enhanced by keeping signals in the SW domain and avoiding frequent interconversions between electrical and SW signals. Our experimental results of the mutual control between SWs and DWs thus facilitate the possibility of using one SW to modulate the transmission of others by reconfiguring the magnetic domain structures.

REFERENCES AND NOTES

1. V. V. Kruglyak, S. O. Demokritov, D. Grundler, *J. Phys. D* **43**, 264001 (2010).
2. A. Khitun, M. Bao, K. L. Wang, *J. Phys. D* **43**, 264005 (2010).
3. B. Lenk, H. Ulrichs, F. Garbs, M. Münzenberg, *Phys. Rep.* **507**, 107–136 (2011).
4. A. V. Chumak, V. I. Vasyuchka, A. A. Serga, B. Hillebrands, *Nat. Phys.* **11**, 453–461 (2015).
5. G. Csaba, Á. Papp, W. Porod, *Phys. Lett. A* **381**, 1471–1476 (2017).
6. Y. Kajiwara *et al.*, *Nature* **464**, 262–266 (2010).
7. Z. K. Wang *et al.*, *Appl. Phys. Lett.* **94**, 083112 (2009).
8. H. Yu *et al.*, *Nat. Commun.* **7**, 11255 (2016).
9. T. Schneider *et al.*, *Appl. Phys. Lett.* **92**, 022505 (2008).
10. S. O. Demokritov *et al.*, *Phys. Rev. Lett.* **93**, 047201 (2004).
11. S.-M. Seo, K.-J. Lee, H. Yang, T. Ono, *Phys. Rev. Lett.* **102**, 147202 (2009).
12. Z. Wang, Y. Sun, M. Wu, V. Tiberkevich, A. Slavin, *Phys. Rev. Lett.* **107**, 146602 (2011).
13. A. Hamadeh *et al.*, *Phys. Rev. Lett.* **113**, 197203 (2014).
14. V. Vlaminck, M. Bailleul, *Science* **322**, 410–413 (2008).
15. R. Hertel, W. Wulfhekel, J. Kirschner, *Phys. Rev. Lett.* **93**, 257202 (2004).
16. C. Bayer, H. Schultheiss, B. Hillebrands, R. L. Stamps, *IEEE Trans. Magn.* **41**, 3094–3096 (2005).
17. S. Macke, D. Goll, *J. Phys. Conf. Ser.* **200**, 042015 (2010).
18. J. S. Kim *et al.*, *Phys. Rev. B* **85**, 174428 (2012).
19. F. J. Buijnsters, Y. Ferreiros, A. Fasolino, M. I. Katsnelson, *Phys. Rev. Lett.* **116**, 147204 (2016).
20. E. Albisetti *et al.*, *Nat. Nanotechnol.* **11**, 545–551 (2016).
21. K. Wagner *et al.*, *Nat. Nanotechnol.* **11**, 432–436 (2016).
22. S. S. P. Parkin, M. Hayashi, L. Thomas, *Science* **320**, 190–194 (2008).
23. P. Pirro *et al.*, *Appl. Phys. Lett.* **106**, 232405 (2015).
24. P. Yan, X. S. Wang, X. R. Wang, *Phys. Rev. Lett.* **107**, 177207 (2011).
25. Detailed discussions are available in the supplementary materials.
26. J.-M. Beaujour, D. Ravelosona, I. Tudosa, E. E. Fullerton, A. D. Kent, *Phys. Rev. B* **80**, 180415(R) (2009).
27. M. Bailleul, D. Olligs, C. Fermon, S. O. Demokritov, *Europhys. Lett.* **56**, 741–747 (2001).
28. V. Vlaminck, M. Bailleul, *Phys. Rev. B* **81**, 014425 (2010).
29. W. Jiang *et al.*, *Phys. Rev. Lett.* **110**, 177202 (2013).
30. L. J. Cornelissen, J. Liu, R. A. Duine, J. Ben Youssef, B. J. van Wees, *Nat. Phys.* **11**, 1022–1026 (2015).
31. N. Loayza, M. B. Jungfleisch, A. Hoffmann, M. Bailleul, V. Vlaminck, *Phys. Rev. B* **98**, 144430 (2018).
32. K.-S. Lee, S.-K. Kim, *J. Appl. Phys.* **104**, 053909 (2008).
33. M. J. Donahue, D. G. Porter, "OOMMF User's Guide, version 1.0" (National Institute of Standards and Technology, 1999).
34. Y. Cheng, K. Chen, S. Zhang, *Appl. Phys. Lett.* **112**, 052405 (2018).
35. X. Wang, G. Guo, Y. Nie, G. Zhang, Z. Li, *Phys. Rev. B* **86**, 054445 (2012).
36. S. Woo, T. Delaney, G. S. D. Beach, *Nat. Phys.* **13**, 448–454 (2017).
37. V. E. Demidov *et al.*, *Nat. Mater.* **11**, 1028–1031 (2012).
38. Z. Duan *et al.*, *Nat. Commun.* **5**, 5616 (2014).
39. J. Han, P. Zhang, J. T. Hou, S. A. Siddiqui, L. Liu, Data from: Mutual control of coherent spin waves and magnetic domain walls in a magnonic device. Version 1, Zenodo (2019); https://doi.org/10.5281/zenodo.3483803.

ACKNOWLEDGMENTS

The simulations were performed on the Engaging Cluster at the Massachusetts Green High Performance Computing Center (MGHPCC). J.H. acknowledges J. Han and H. Wang for help with device fabrication and SEM imaging. **Funding:** This work was supported by AFOSR under award FA9550-19-1-0048 and the National Science Foundation under award ECCS-1653553. **Author contributions:** L.L. proposed and directed the study. J.H. prepared the samples and carried out the measurements, with help from S.A.S. P.Z. conducted micromagnetic simulations. J.T.H. helped with the measurement setup. J.H., P.Z., and L.L. analyzed the data and wrote the manuscript. All authors commented on the manuscript. **Competing interests:** The authors declare no competing interests. **Data and materials availability:** All data shown in the main text and the supplementary materials are deposited in the Zenodo public repository (*39*). The micromagnetic simulations are performed by using the open-source code OOMMF (Object Oriented Micromagnetic Framework) (*33*).

SUPPLEMENTARY MATERIALS

science.sciencemag.org/content/366/6469/1121/suppl/DC1
Materials and Methods
Supplementary Text
Figs. S1 to S13
References (*40*–*71*)

24 May 2018; resubmitted 21 November 2018
Accepted 4 November 2019
10.1126/science.aau2610

Science

Mutual control of coherent spin waves and magnetic domain walls in a magnonic device

Jiahao Han, Pengxiang Zhang, Justin T. Hou, Saima A. Siddiqui and Luqiao Liu

Science **366** (6469), 1121-1125.
DOI: 10.1126/science.aau2610

Toward magnonic devices

The field of magnonics aims to use spin waves (SWs) and their associated quasiparticles—magnons—as carriers of information. Compared with the movement of charge in conventional electronics, a major advantage of SWs is reduced Joule heating. However, SWs are trickier to direct and control. Two groups now go a step further toward magnon-based devices. Han *et al.* show that in multilayer films, domain walls can be used to change the phase and magnitude of a spin wave. Wang *et al.* demonstrate how magnon currents can be used to switch the magnetization of an adjacent layer.

Science, this issue p. 1121, p. 1125

Science (print ISSN 0036-8075; online ISSN 1095-9203) is published by the American Association for the Advancement of Science, 1200 New York Avenue NW, Washington, DC 20005. The title *Science* is a registered trademark of AAAS.